京都大学防災研究所年報 第 49 号 C 平成 18 年 4 月
Annuals of Disas. Prev. Res. Inst., Kyoto Univ., No. 49 C, 2006

Analysis and Prediction of Anomalous Weather and Atmospheric Hazards

Hiromasa KAWAI, Tatsuya IWASHIMA, Hirohiko ISHIKAWA,
Takashi MARUYAMA, Hitoshi MUKOUGAWA,
Mitsuaki HORIGUCHI, Takao IGUCHI and Tokihiko ARAKI

Synopsis

This paper describes the analysis of various phenomena related with anomalous weather and its hazards, which consists of three parts. The first part describes a new method for obtaining initial perturbations appropriate to the ensemble forecast of the intraseasonal variability in the tropics, which was developed using the operational numerical weather forecast system of the Japan Meteorological Agency. The obtained initial perturbations have spatial structure similar to eastward propagating dry Kelvin wave with phase speed of 30 m/s. The second part shows a numerical method to simulate strong wind fields over complex topography during typhoon. for investigating the strong wind characteristics and predicting wind hazards. The PSU/MM5 and LES were used for the calculation of meso and micro-scale unsteady wind fields. The last part describes the results of the analyses using FY"C data for the research and prediction of Japanese abnormal weather, especially in Baiu season, which came into official operation in May, 2005 and observes a wide area of Monsoon Asia extending from Saudi Arabia to Japan from 104E, just above Singapore..

Keywords: anomalous weather, Madden-Julian Oscillation, JMA one-month ensemble forecast system, initial perturbations for tropical intraseasonal oscillation numerical simulation, strong wind, complex topography, typhoon, MM5, LES, Feng-Yun 2C, MTSAT, MODTRAN

1. Predictability of Madden-Julian Oscillation in the Tropics

1.1 Introduction

Madden-Julian Oscillation (MJO) is the most dominant component in theintraseasonal variability in the tropical atmosphere (e.g., Madden andJulian, 1994). MJO has a period of 30-60 days, and is characterized byeastward propagating anomalous convective activity around the globe. MJO also accompanies characteristic circulation anomaly, and is closely related to the onset and the variation of the Australian Monsoon as well as the the Asian Monsoon (Yasunari, 1979; Lau and Chan, 1986; Hendon and Liebmann, 1990). Nakazawa (1986) also showed that MJO is closely connected with the generation and the development of the tropical cyclone and typhoon. Recent observational study also showed that MJO affects the weather around Japan in winter as well as the well known teleconnection pattern in the North Pacific. Moreover, it was indicated that the forecast of the extratopical circulation tends to become skillful when the forecast skill of MJO in the tropics is above the average. Thus, MJO plays an important role in the generation and prediction of extreme weather in the extratropics including Japan.

However, general circulation models and numerical weather prediction models has not succeeded to reproduce several properties of observed MJO (e.g., Slingo et al., 1996). Jones et al. (2000) indicated that MJO-like variations appeared in their numerical model have smaller amplitude and shorter period compared with the observation. It is also found that the forecast skill of MJO by National Centers for Environmental Prediction (NCEP) medium-range weather forecast model is only significant for the lead time of 5-7 days (Chen and Alpert, 1990; Lau and Chang, 1992; Hendon et al., 2000; Jones et al., 2000).

On the other hand, it is still controversial for the relationship between the predictability of MJO and the activity and phase of MJO itself. For example, Jones et al. (2000) indicated that the prediction of MJO becomes slightly skillful when the convection associated with MJO becomes active by diagnosing zonal winds in the upper troposphere of the NCEP medium-range forecasts. Boer (1995), however, showed that the predictability of MJO is almost independent of its activity. Moreover, Hendon et al. (2000) and Lo and Hendon (2000) indicated that the prediction of MJO becomes skillful when MJO is inert using predicted streamfunction by the forecast system of European Centre for Medium-Range Weather Forecasts (ECMWF). Kubota et al. (2005) also showed by using one-month forecast data of Japan Meteorological Agency (JMA) that the reproduced amplitude of MJO is smaller than the observation, and a consistent relationship between the predictability of MJO and its phase does no seem to exist.

1.2 Revised Breeding Method

Kubota et al. (2005) also indicated that the initial perturbation of the perturbations of JMA one-month ensemble forecast system is quite large compared with MJO itself, and their horizontal structure is not also suitable to access the predictability of MJO. Thus, Climate Environment Research Group of DPRI are now proceeding a joint research project with Climate Prediction Division of JMA to access the predictability of MJO using operational one-month ensemble prediction system of JMA. In this paper, we report the preliminary results of the joint research project on producing suitable initial perturbations for the tropical intraseasonal oscillation using operational numerical weather prediction model (GSM) of JMA.

For this purpose, we have revised the Breeding of Growing Mode (BGM) method (Toth and Kalnay, 1993; 1997) which has been used to produce initial perturbations for the one-month prediction of JMA. The BGM method which was originally developed in NCEP produces initial perturbations using the following procedure. Firstly, we conduct 12-hr forecast without initial perturbation (control forecast), and also 12-hr forecast with arbitrary initial perturbations (perturbed forecast). From the difference between the perturbed and the control forecasts, we obtain grown small perturbations. Secondary, usingGram-Schmidt orthogonalization method, a set of normalized and orthogonalized perturbations is computed from the grown perturbations. Thirdly, we repeat the first procedure from the obtained set of perturbations, and finally obtain a set of orthogonal growing perturbations at every initial time. The obtained set of orthogonal growing perturbations is similar to the Lyapunov vector. The above sequence will be referred to as the perturbation cycle. In the operational perturbation cycle of JMA, the norm of the perturbation is defined by the area-averaged root-mean squared variation of the geopotential height of the perturbation at 500 hPa northward of 20S. The magnitude of the norm is also set to be 14.5% of the climatic variability of the geopotential height at 500 hPa..

In this study, in order to obtain suitable small perturbations for MJO, we have revised the perturbation cycle of JMA as follows: The norm of the perturbation is defined by using the kinetic energy associated with horizontal winds at 200 hPa (referred to as KE200) in

the tropics, or the vector potential at 200 hPa (referred to as X200). Since the obtained results are almost the same for the norm of KE200 and X200, we will report the results using KE200. The magnitude of the norm evaluated within the tropics from 20S to 20N was set to be 14.5% of the climatic variability as in the operational breeding cycle. Moreover, the amplitude of the perturbation poleward of 20S and 20N was reduced to zero by operating a Gaussian function. The tapered perturbations would effectively reduce the vigorous baroclinic instability prevailing in the extratropics, and we could obtain perturbations associated with the tropical atmospheric circulation..

The perturbation cycle was done by changing the period of the time-integration, i.e. 12 hr which is the same as in the operational cycle and 24 hr. The initial perturbation for the perturbation cycle was given by the operational initial perturbation of 1p and 2p at 1200UTC 15 October 2003, and was conduced through 1200UTC 31 January 2004. The initial perturbations 1p and 2p have the largest growth rate among the initial perturbations and are orthogonal with each other. In the following, the perturbation cycle with 12 hr (24 hr) integration period starting from 1p will be referred to as KE12h1p (KE24h1p). The cycle from 2p will be KE12h2p and KE24h2p. In this study, we did not perform the orthogonalization at every 1200UTC. This is because we could suggest the existence of an unstable mode associated with MJO if the structure of the

obtained perturbations from 1p and 2p becomes similar due to the dominance of a growing mode.

The numerical weather prediction model used in this experiment was GSM0305 with the resolution of T106L40. Prognostic Arakawa-Schubert (Randall and Pan, 1993) scheme was used for the parameterization of the cumulus convection. The output data was given by grid point values with horizontal resolution of 1.25 degree.

1.3 Results

During the experimental period, the activity of MJO is very high from early December to January. Fig. 1 shows the anomaly of the Outgoing Longwave Radiation (OLR) during this period, while Fig. 2 is for the anomaly of X200 anomaly. MJO becomes active in December, and the positive anomaly of X200, corresponding to the region of active convection, slowly propagates eastward over the Indian Ocean in the first half of December and the Pacific in the last half of December. The convection over the eastern Indian Ocean and the western Pacific becomes active associated with the eastward propagation of MJO as shown by the region of negative anomaly of OLR in Fig. 1. After that, the convection is strongly suppressed over the eastern Indian Ocean and Indonesia from 10 January to 25 January. It is also found that the anomalous easterly winds which is prevailed in the lower troposphere over the western Pacific in late November also propagate eastward in association with the region of the convective region. Anomalous westerlies westward of the convective region also propagate eastward.

Fig. 3 shows the longitude-time cross section of the latitudinally averaged X200 of the obtained perturbation from 10S to 10N by improving the operational perturbation cycle of JMA for MJO. The four panels in this figure show perturbations with 12 hr cycle and 24 hr from the initial perturbations of 1p and 2p. First of all, it has to be stressed that the obtained perturbation has a small amplitude compared with the operational one. The small amplitude is suitable for the ensemble prediction of MJO. We also see some differences in the structure of the perturbation of 12 hr and 24 hr perturbation cycle. In particular, for the perturbation by 24 hr cycle, the eastward movement of X200 is evident, and the the variation of X200 is larger than the perturbation with 12 hr cycle. Moreover, the similarity of the horizontal structure between 1p and 2p perturbations with 12 hr cycle is weak compared with the perturbation of 24

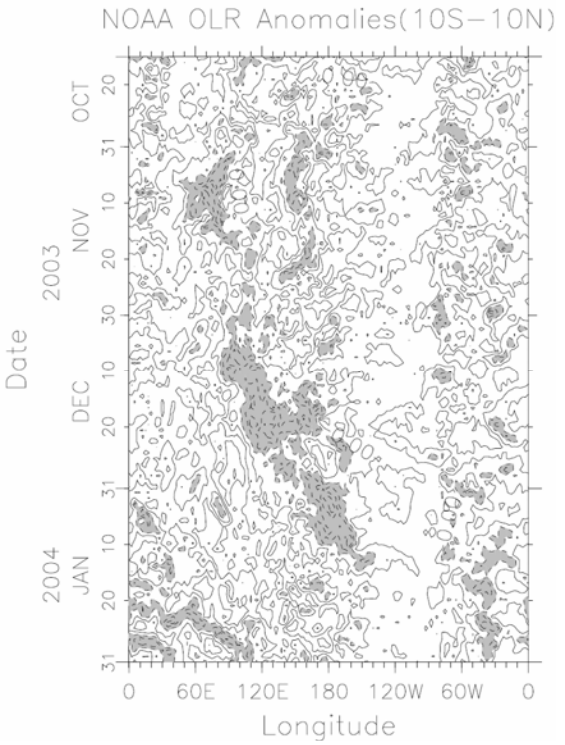

Fig. 1. Time-longitude cross section of OLR anomaly observed by NOAA from 16 Oct. 2003 to 31 Jan. 2004. Shaded regions are where values are smaller than 20W/m^2.

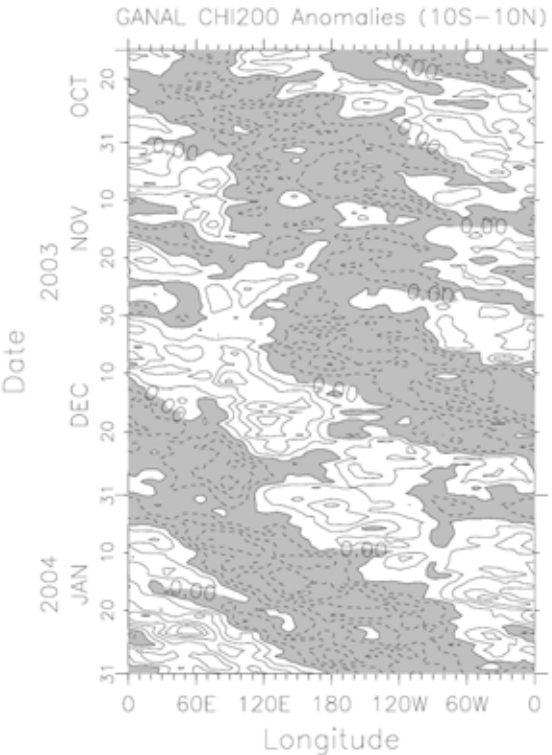

Fig. 2. Time-longitude cross section of X200 anomaly of GANAL from 16 Oct. 2003 to 31 Jan. 2004. Negative values are shaded. Contour interval is 4×10^6 m^2/s.

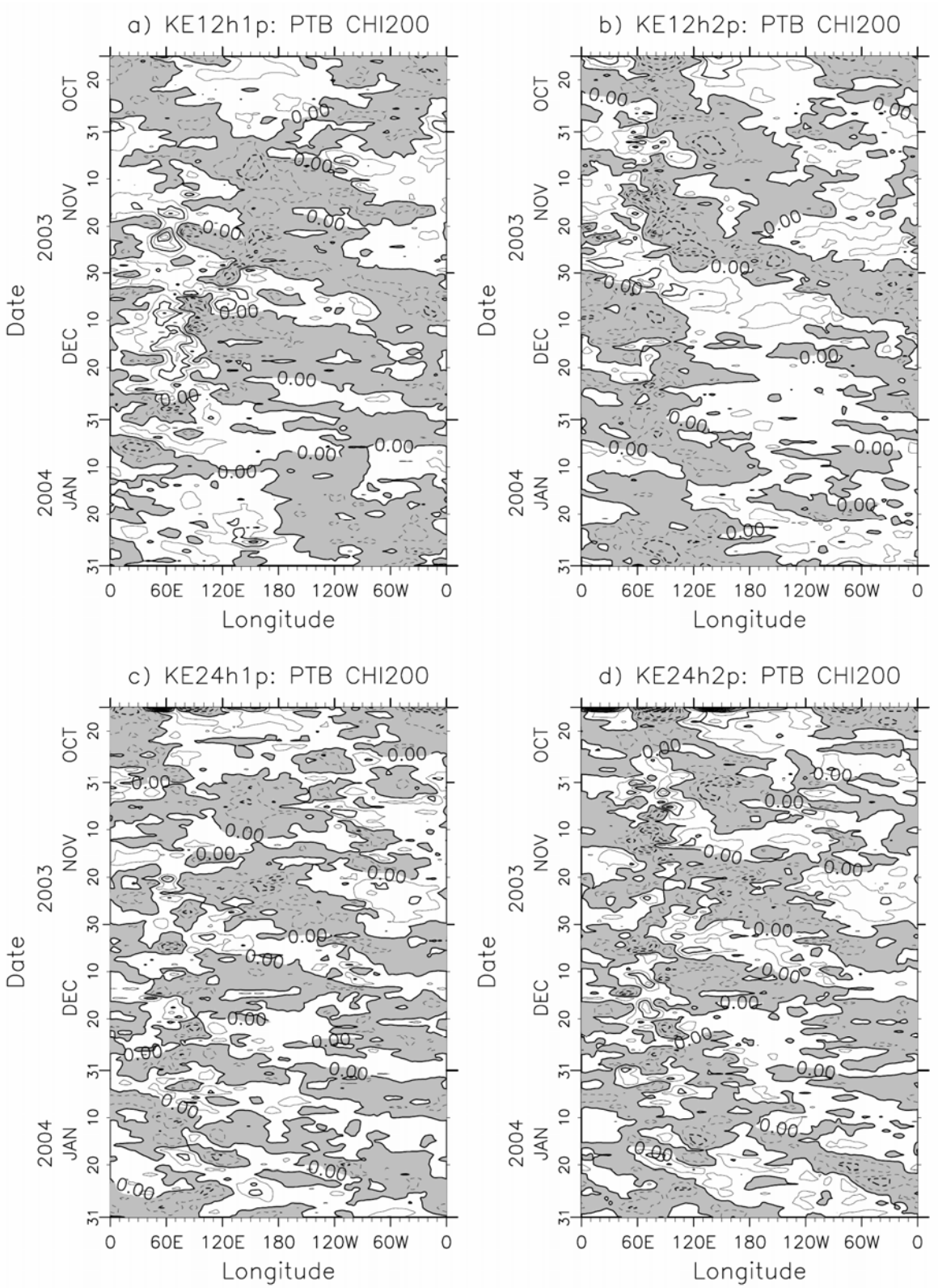

Fig. 3. Time-Longitude cross section of X200 of the perturbation for (a) KE12h1p, (b) KE12h2p, (c) KE24h1p, and (d) KE24h2p. The values are averaged over the region from 10S to 10N. Contour interval is 8×10^5 m^2/s.

hrcycle. For the 24 hr cycle, it is found that the similarity of the horizontal structure of 1p and 2p perturbation is significant by computing the anomalous correlation between them (not shown). This fact suggests an emergence of dynamically unstable mode associated with MJO for 24 hr cycle. We also conducted a time-space spectral analysis for X200 perturbation in the tropics (from 10S to 10N) to obtain dominant component

in the variability. For the perturbation with 12 hr cycle, zonal wavenumber 1 component has a peak amplitude, but the spectral shape is rather red, and the stationary components have the maximum amplitude (not shown). On the other hand, for the perturbation with 24 hr cycle, eastward propagating zonal wavenumber 1 component with a period around 15~20 days has a peak amplitude for both 1p and 2p initial perturbation (not shown). The horizontal structure of the perturbation suggests that the perturbation could corresponds to the eastward propagating dry Kelvin wave (Milliff and Madden, 1996; Bantzer and Wallace, 1996) in the tropical region with a phase speed of 30 m/s.

The growth rate of the perturbation was also examined (not shown) by computing the amplitude growth of the perturbation during the perturbation cycle (not shown). From this analysis, it is suggested that the perturbation has a much smaller growth rate compared with the vigorous baroclinic instability in the extratropics, and might be weakly damped. However, we need further analysis to discuss the dynamical stability of MJO.

1.4 Concluding Remarks

In order to examine dynamical predictability of the intraseasonal variability in the tropics, we devised a new breeding method for initial perturbations appropriate to the ensemble forecast of the intraseasonal variability in the tropics using the operational numerical weather forecast system of the Japan Meteorological Agency. The obtained initial perturbations have spatial structure similar to the eastward propagating dry Kelvin wave with phase speed of 30 m/s. The growth rate of the perturbation is very small compared with the baroclinic instability in the extratropics. We are now conducting a set of ensemble hidcast experiments by using the operational JMA weather prediction system with the obtained initial perturbations in this study to assess the predictability of MJO.

1.5 Acknowledgments

We would like to thank all the members in Numerical Prediction and Climate Prediction Divisions in JMA for providing us 1-month forecast data sets of JMA. The GFD-DENNOU Library was used for the graphics.

2. A Trial of Numerical Simulation on Strong ind Fields over complex topography during Typhoon

2.1 Introduction

The strong wind during typhoon is characterized not only by meteorological mechanism but also by topographical effect. Therefore we had better to incorporate both effects into the simulation of strong wind fields. The calculation also includes various scales of phenomena from meso-scale which covers the Japanese islands to fine-scale of local topography such as ground up-down and surface roughness. Here we examined a numerical method with The PSU/MM5 model (Dudhia, 1993 ; hereafter abbreviate MM5) for meso-scale regions and the Large Eddy Simulation (hereafter abbreviate LES) for local topography. The calculated results will be compared with the observed records and the field investigation of damage to the houses and plants. The applicability of wind hazard prediction is examined.

2.2 Over view of simulating method

The governing equations for fluid and various quantities were discretized by the finite difference method for numerical calculation. The MM5 model was used for the calculation of meso-scale wind fields and the RIAM-COMPACT（Uchida et.al, 2004） based on LES was used for fine scale of local topography. The wind fields during Typhoon Songda in 2004 were examined by using the multi-scale regions from the meso-scale region covered the Japanese islands to the local topography of Miyajima island in Hiroshima Bay as

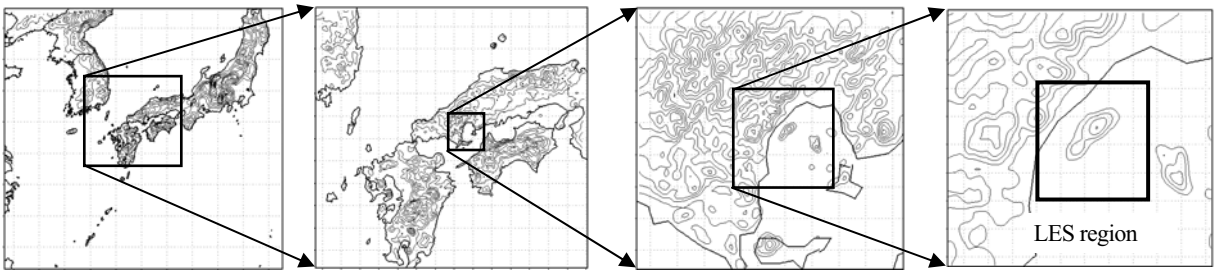

a .Region1 : 2151×2151 km^2　b .Region3 : 630×630 km^2　c .Region3 : 90×90 km^2　d .Region4 : 30×30.km^2

Fig.4　Calculation regions for MM5

shown in Figure 4. Unsteady strong wind field was calculated by LES with fine mesh. Figure 5 shows the configuration of mesh discretization around Miyajima island which resolves the detailed topography near Itsukushima shrine.

2.3 Calculated results

(1) Simulation of typhoon

Typhoon Songda was simulated from September 6 at 21:00 JST to September 7 at 21:00 JST. The passage of calculated center of the typhoon is almost equivalent as shown in Figure 6 but it a little bit slowly proceeds than the real typhoon. The lower pressure of typhoon center was predicted after September 7, 12:00 JST as shown in Figure 7. The distribution of wind speed near the ground shows the strong wind fields in Figure 8 which caused severe damage in Yamaguchi and Hiroshima prefecture along sea shore. The comparison with the measured records in Figure 9 presents good prediction of wind direction. The temperature correlated well near sea at Kure but showed higher value in urban area at Hiroshima. Higher wind speed was obtained in calculation. The time variation of wind speed had same trend except at Miyajima. This discrepancy of wind direction and speed is supposed to be caused by the location of measuring apparatus and influenced by the surrounding local topography. To clarify the wind characteristics over complex terrain the unsteady flow simulation with fine mesh was conducted by using LES.

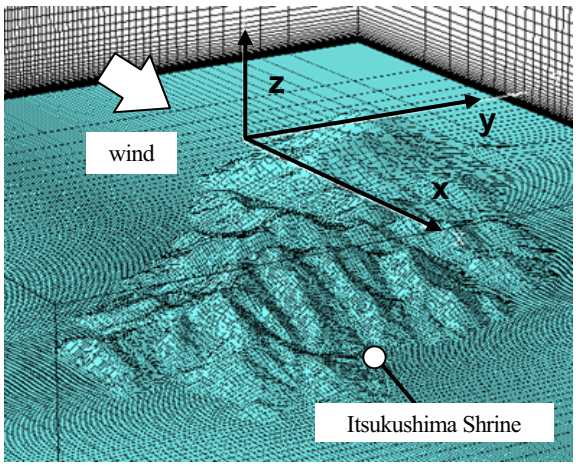

Fig.5 Calculation region for LES

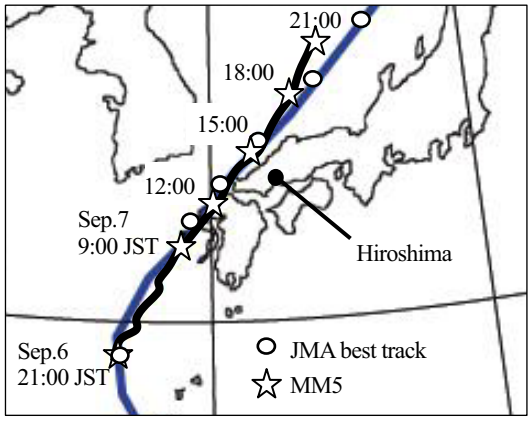

Fig.6 Track of typhoon center

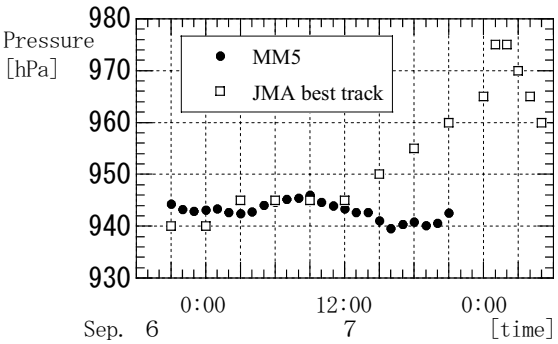

Fig.7 Variation of typhoon center pressure

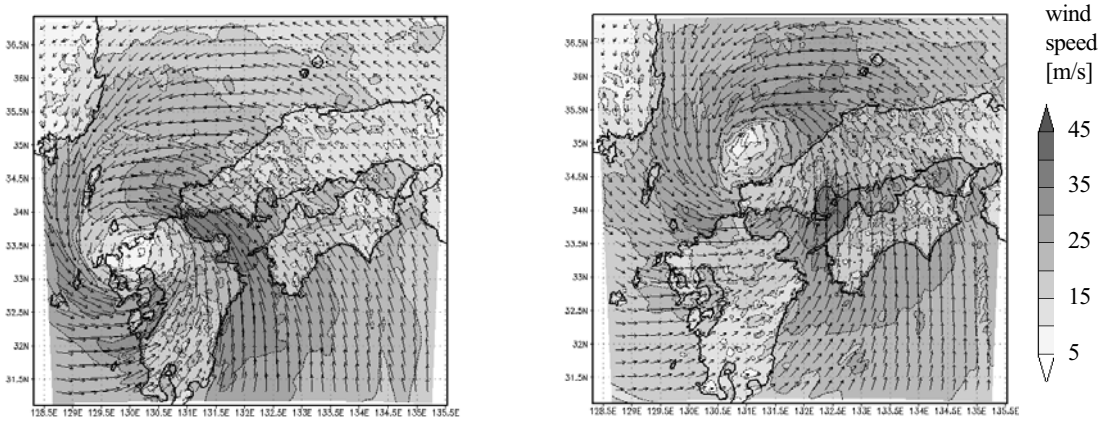

a . 11:00, Sep. 7 b . 14:00, Sep. 7

Fig.8 Contour map of horizontal wind speed at 10m over the ground and sea simulated by MM5 in Region 2

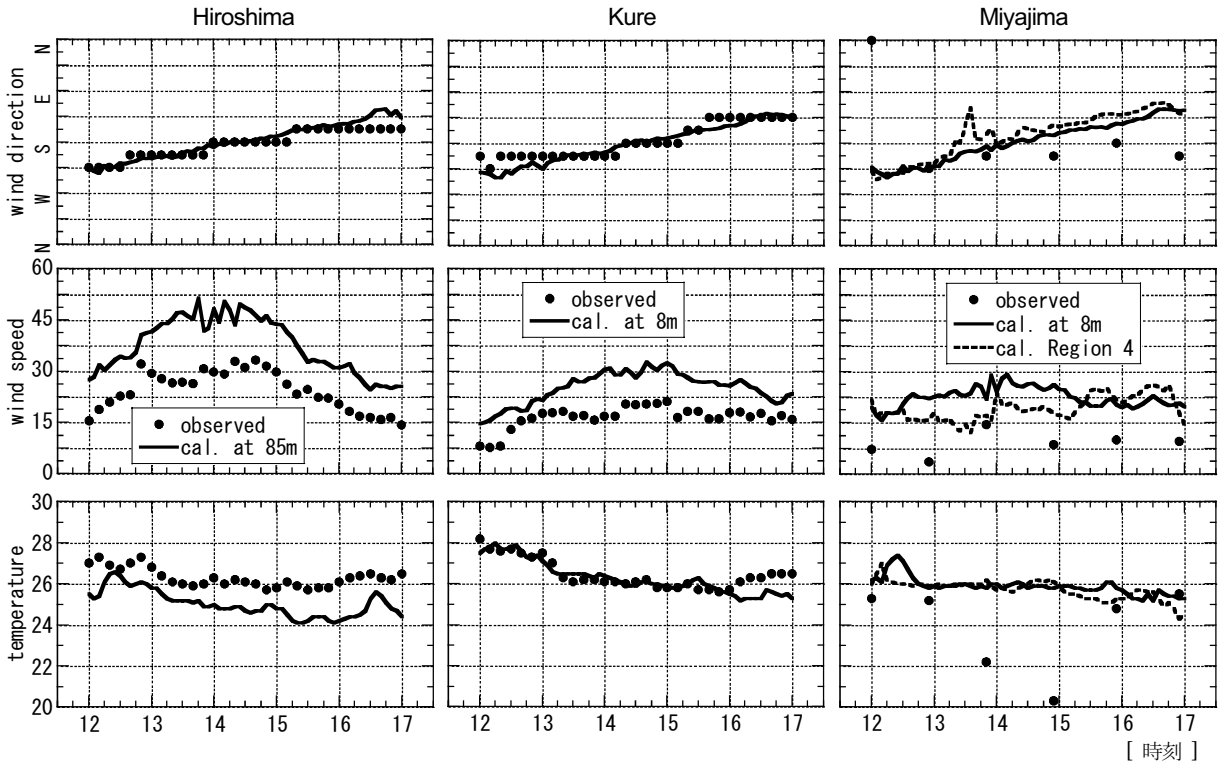

Fig.9 Comparison of simulated results of MM5 in region 3 with observed data around Hiroshima bay

(2) Local wind field around Itsukushima shrine

Itsukushima shrine is located at the end of north-east inlet of Miyajima island as shown in Figure 10. It is surrounded by the steep slopes of southern mountains in Photo 1 and a valley is approaches to the shrine from the col between the mountains. According to the reports of Typhoon Songda （Maruyama et.al, 2005）, there were many damage to houses and plants around the shrine caused by the wind. The evidences and the damage testify that the strong wind frequently changed its direction in a short time. The simulation by using LES with fine mesh shown in Figure 2 was done. Three cases with different inlet wind direction were calculated at 13:00, 14:00 and 15:00 JST on September 7 as shown in Figure 11. The areas with reversal mean wind direction near the ground, painted dark, change according to the inlet wind direction. The calculation was conducted with no temperature change. This means the atmosphere is neutral and strong wind condition. At 14:00 JST, when the strong wind damage around the shrine was reported, the mean wind blew along the valley and no reverse wind region was obtained in the section along the line A-B in Figure 8 b from the col to the shrine as shown Figure 12.

The LES simulation results the unsteady wind field. Figure 13 shows the calculated wind at Itsukushima

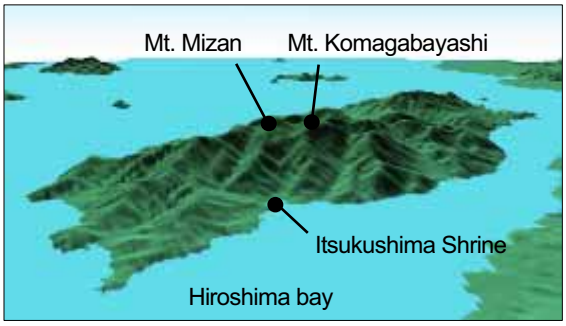

Fig.10 Bird's-eye-view of Miyajima Island from the north

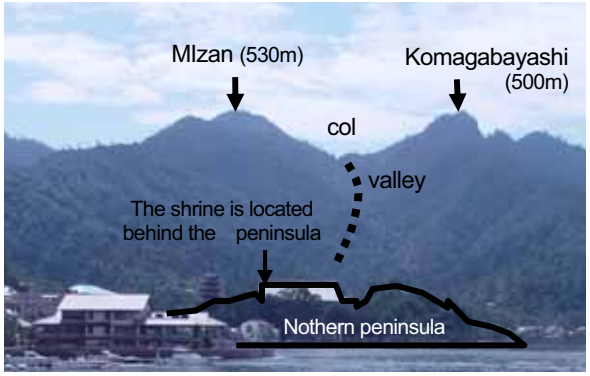

Photo 1. View of mountains and valleys to the south of Itsukushima Shrine from the northern port

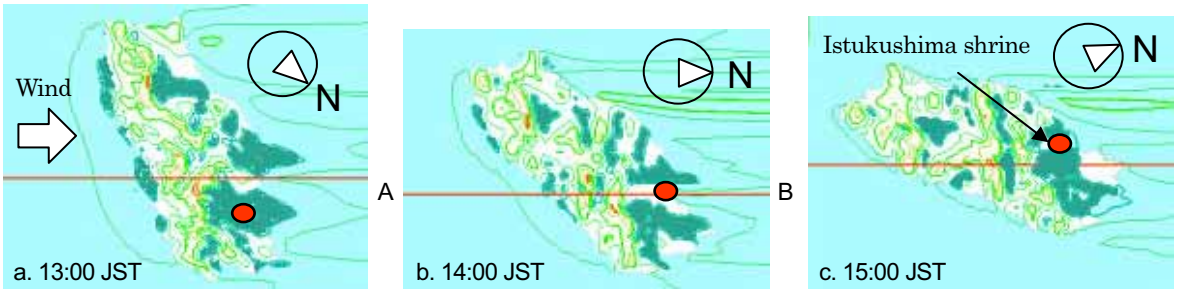

Fig. 11 LES results of mean wind field around Miyajima Island at 10m from the ground and the sea. The regions where the wind direction is reverse to the inlet wind are shown dark.

shrine and at Daishouin temple located on the middle of the valley. The wind at the temple blows from the col to the shrine but occasionally directs upward. This coincide with the witness of the priest who observed the wind flow during the typhoon passage at the tmple. On the other hand, the wind at Itsukushima shrine indicates rapid change. The wind blows not only from the south but also from the west, from the east and from the north. The wind from the south is relatively stronger than the wind blows from other directions. The instantaneous wind vector distributions near the ground are shown in Figure 14.

(3) Wind hazard prediction

We obtained the maximum wind speed map in Figure 15 from the meso-scale simulation using the MM5. This shows good correlation to the strong wind and the high damage rate areas shown in Figure 16. This means that the simulation method will be applicable to the wind hazard study.

2.4 Conclusion

We examined a numerical method using the PSU/MM5 model and the RIAM-COMPACT based on Large Eddy Simulation to simulate strong wind fields above complex topography. The calculated results during Typhoon Songda in 2004 were caluculated numerically.

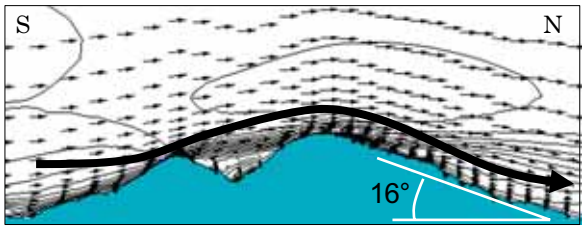

Fig. 12 Wind velocity vectors on the vertical plane along the line A-B shown in Fig.8b.

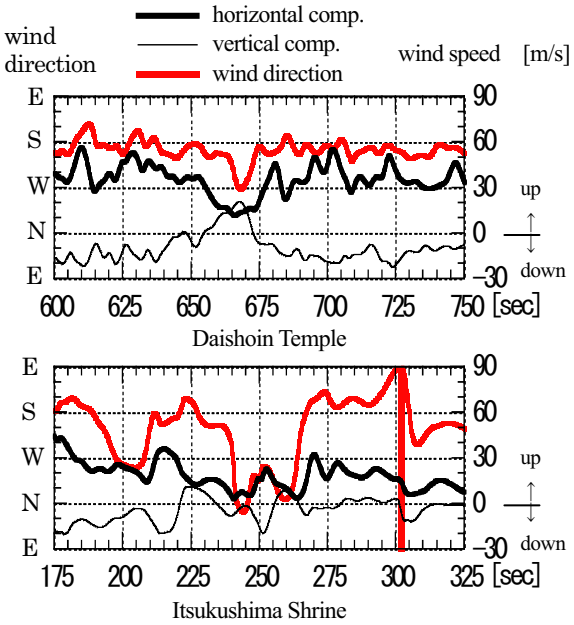

Fig. 13 Time variation of wind velocities by LES near the ground at 10m

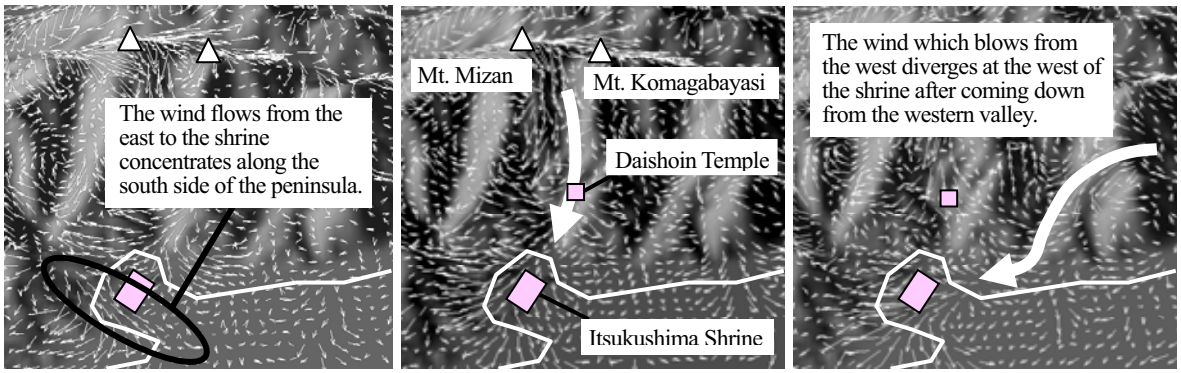

a . East wind at the shrine b . South wind at the shrine c . West wind at the shrine

Fig. 14 Instantaneous wind velocity vector fields around Itsukushima Shrine at 10m from the ground and the sea.

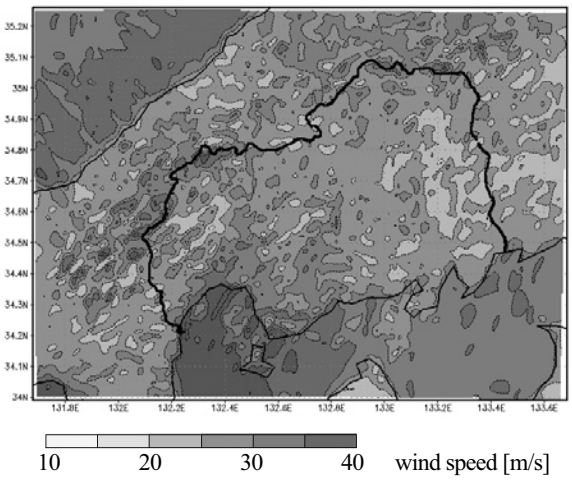

Fig.15 Contour map of maximum mean wind speed at 10m calculated by MM5

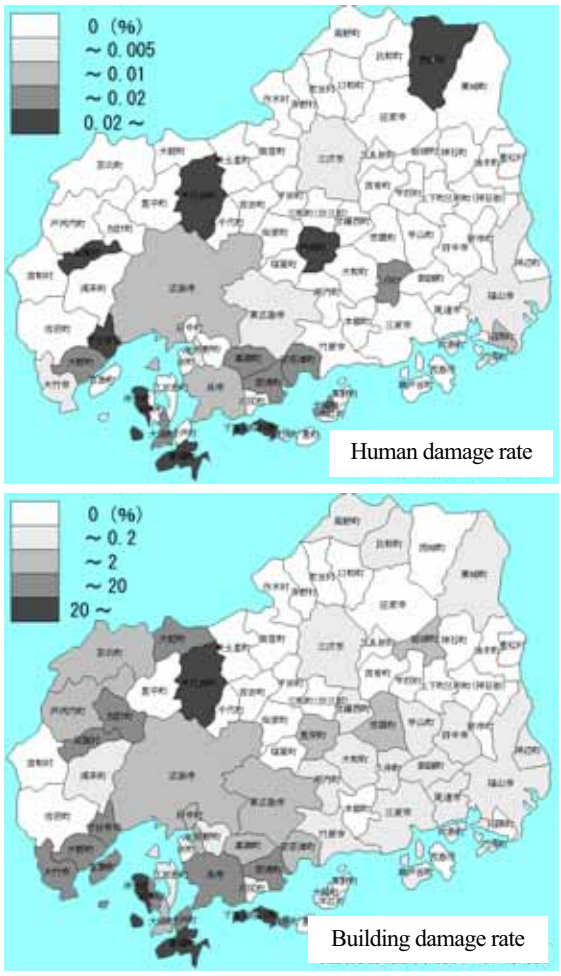

Fig. 16 Distribution of damage rate in Hiroshima prefecture.

The strong winds those passed over the sea surrounded by the lands causing the damage along sea shores were simulated in the meso-scale regions. Unsteady wind fields were computed in the fine region around Itsukushima Shrine in Miyajima island. The simulated local wind characteristics caused by the topography show good correlation to the observed records, the field investigation of damage and the witnesses during the typhoon. The calculated maximum wind speed map was well correlated to the distribution of houses and human damage rate in Hiroshima Prefecture.

3. Monitoring of Asian weather from Chinese Geostationary Satellite, Feng-Yun 2C evere storm and the related study

3.1 FY2C Data

Chinese operational geostationary meteorological satellite, Feng-Yun 2C (FY2C), came into official operation in May, 2005. FY2C observes a wide area of Monsoon Asia extending from Saudi Arabia to Japan from 104E, just above Singapore. At the Severe Storm and Atmospheric Environment Section of Atmospheric and Hydrospheric Research Division, the data from FY2C is received and archived since January 23, 2005. Before the official operation, we observed that the orbit was a little bit fluctuating and the calibration was changing, but after May the data are well transmitted.

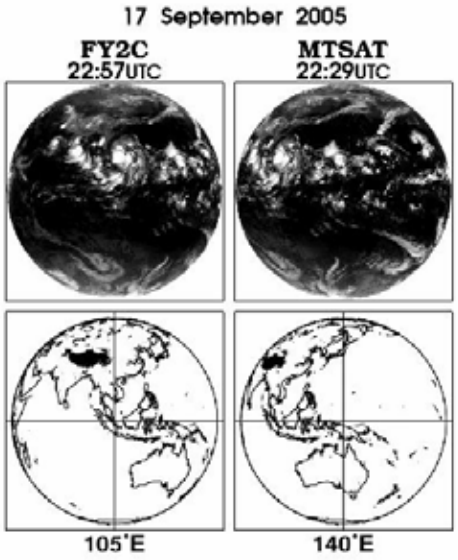

Fig.17 Full-disc image of FY2C and MTSAT

The use of FY2C data is expected to contribute to the research and prediction of Japanese abnormal weather, especially in Baiu season, since the Baiu front is the eastern end of a systematic polar front extending from the Bay of Bengal. Figure 17 compares the difference of images observed from FY2C and MTSAT_1R, the new Japanese geostationary meteorological satellite. It is understood that the MTSAT is useful in detecting the

tropical cyclones, whereas the FY2C is suitable for the detection of mid-latitude disturbances which are generally propagating from west to east. Furthermore, FY2C is the most suitable to detect the cloud activity and the accompanied precipitation in the monsoon Asia. In this area, the Indian meteorological satellite is in operation at ???E but the data are scrambled, whereas the data from the FY2C is transmitted by HiRID (a expanded version of SVISSR) format.

3.2 Data Quality

In prior to use the FY2C data it is necessary to confirm the quality of the data. The validity of the data is checked by the comparison of FY2C and MTSAT observation. It is also confirmed by theoretical calculation of radiation transfer code, MODTRAN.

Since atmospheric constituents absorb radiation transmitted from the earth surface before reaching satellite, the observed radiance depends on the optical depth of atmosphere between the objects and the radiometer. Therefore, we select a target region shown in Figure 18 for comparison where the distance from the satellite is almost the same.

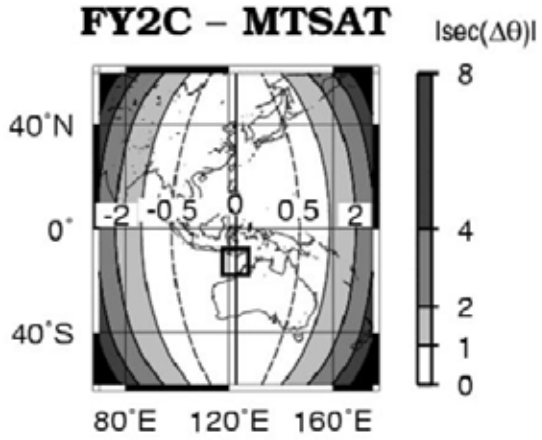

Fig.18 Zenith angle to the satellite. The rectangular area between Australia and Indonesia is used in the comparison in Fig.4.

The observed radiance is also dependant on the filter function of radiometers mounted on the satellite. The filter function of FY2C and MTSAT is compared in the Figure 19. The filter functions of MTSAT are generally sharper than those of FY2C. In order to clarify this effect, theoretical value of Tbb is computed using a radiation transfer code, MODTRAN, considering the filter function. In the theoretical calculation the sea surface temperature is taken form the NOAA SST100 dataset

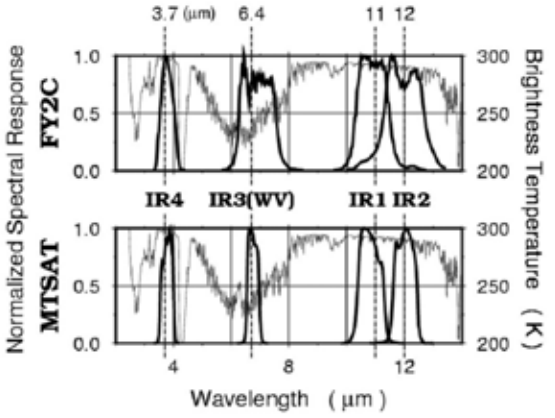

Fig.19 Comparison of filter functions of MTSAT and FY2C.

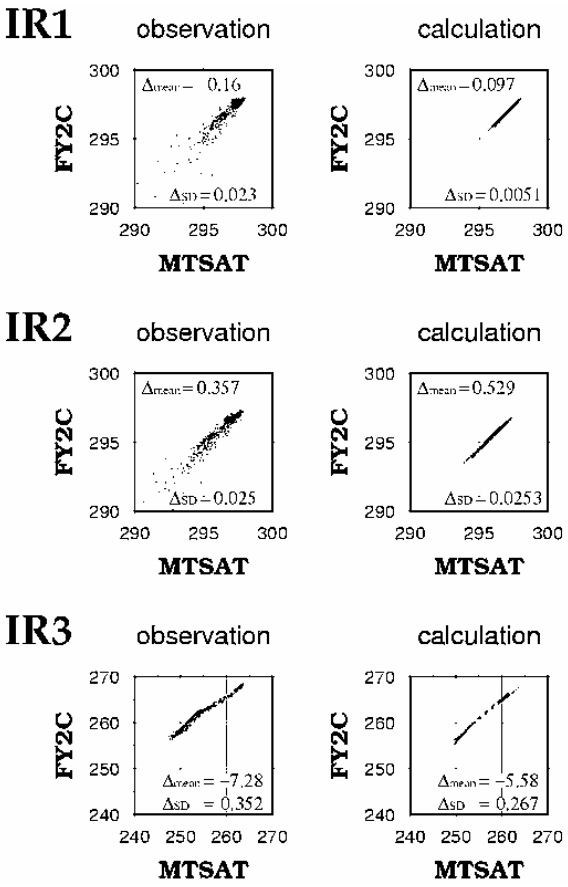

Figure 20 Comparison of Tbb observed (left) and computed (right) for three infrared bands, IR1 (11μm), IR2 (12μm) and IR3 (6.7μm).

and the typical atmospheric profiles in tropics and mid latitudes are used. The sea surface emissivity is assumed as 0.98. The results are shown in Figure 20. The left hand scatter diagrams are comparisons of observed Tbb (Equivalent Black Body Temperature) and the right hand scatter diagrams are comparison for theoretical calculation. It is seen that the Tbb observed by the FY2C

is lower than that of MTSAT by 0.16K in IR2 (11 μ m band) and 0.4 K in IR2 (12 μ m band), whereas in the water vapor channel, IR3 (6.7 μ m band), higher by 7K. These features are almost consistent with the result of theoretical simulation. The quality of split window channels (11 μ m and 12 μ m) is almost identical to that of MTSAT. The water vapor channel (6.7 μ m) is also available for qualitative analysis.

3.3 Application

As an application of the FY2C data, we first use the FY2C data to retrieve surface temperature over the Tibetan Plateau, which was retrieved using GMS data before (Oku et al. 2004). An example is shown in Figure 21. The data will also be used to monitor the convective activity and the tropical storm in the monsoon Asia, where extreme weather conditions sometimes cause serious disaster. Figure 22 shows a tropical storm in the Bay of Bengal, which is proceeding toward Myanmar. It is also seen that a cloud area extends to the Japan from the Bay of Bengal.

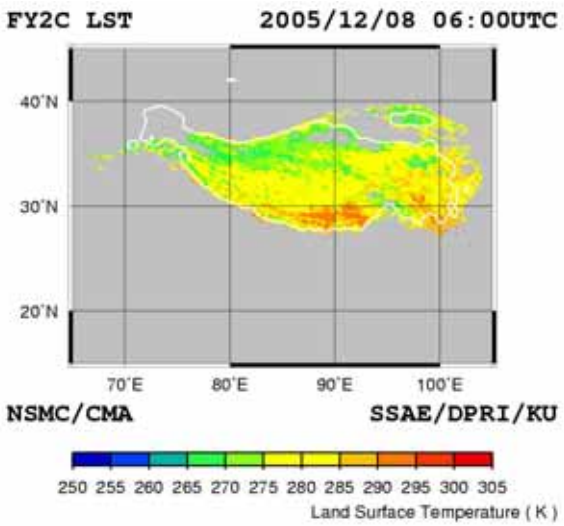

Figure 21 Land surface temperature retrieved from the FY2C infrared data.

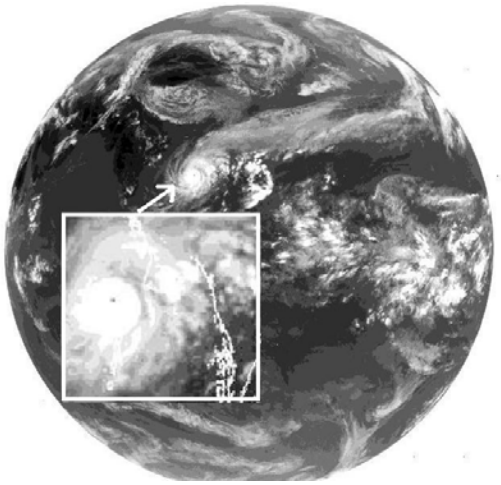

Figure 22. Full disc image on April 28, 2006 10UTC. A strong cyclone is seen in the Bay of Bengal. A cloud band is extending to the east.

References

Bantzer, C. H., and J. M. Wallace, 1996: Intraseasonal variability in tropical mean temperature and precipitation and their relation to the tropical 40-50 day oscillation. J. Atmos. Soc., 53, 3032-3045.

Boer, G. J., 1995: Analyzed and forecast large-scale tropical divergent flow. Mon. Wea. Rev., 123, 3539-3553.

Chen, T-C., and J. C. Alpert, 1990: Systematic errors in the annual and intraseasonal variations of the planetary-scale divergent circulation in NMC medium-range forecasts. Mon. Wea. Rev. 118, 2607-2623.

Dudhia, J.（1993）: A nonhydrostatic version of the Penn State-NCAR meso-scale model: Validation tests and simulation of an Atlantic cyclone and cold front, Mon. Wea. Rev., 121, pp. 1493-1513.

Hendon H. H., B. Liebmann, M. Newman, and J. D. Glick, 2000: Medium-range forecast errors associated with active episodes of Madden-Julian Oscillation. Mon. Wea. Rev., 128, 69-86.

Hendon, H. H., and B. Liebmann, 1990: A composite study of onset of the Australian summer monsoon. J. Atmos. Soc, 47, 2227-2240.

Jones, C., D. E. Wailser, J.-K. E. Schemm, W. K. M. Lau, 2000: Prediction skill of the Madden and Julian Oscillation in dynamical extended range forecasts. Clim. Dynamics, 16, 273-289.

Kubota, T., H. Mukougawa, and T. Iwashima, 2005: Predictability of Madden and Julian oscillation in JMA one-month forecasts (in Japanese). Annuals of Disas. Prev. Res. Inst., Kyoto Univ., 48B, 475-490.

Lau, K.-M., and P. H. Chan, 1986: Aspects of the 40-50 day oscillation during the northern summer as inferred from outgoing longwave radiation. Mon. Wea. Rev., 114, 1354-1367.

Lau, K.-M., and F. C. Chang, 1992: Tropical intraseasonal oscillation and its prediction by the NMC

operational model. J. Climate, 5, 1365-1378.

Lo, F., and H. H. Hendon, 2000: Empirical extended-range prediction of the Madden-Julian Oscillation. Mon. Wea. Rev., 128, 2528-2543.

Madden, R. A. and P. R. Julian, 1994: Observation of the 40-50 day tropical oscillation. A review. Mon. Wea. Rev., 122, 814--837.

Maruyama, T., Kawai H., Masuda K., Tamura Y. and Matsui M., （2005）: Investigation of Damage to itsukushima shrine by Typhoon 0418, Journal of Wind Engineering, No.102, pp. 49-56.

Milliff, R. F. and R. A. Madden, 1996: The existence and vertical structure of fast, eastward-moving disturbance in the equatorial troposphere. J. Atmos. Soc., 53, 586--597.

Nakazawa, T., 1986: Intraseasonal variations of OLR in the Tropics during the FGGE year. J. Meteor. Soc. Japan, 110, 427-441.

Oku,Y, and H. Ishikawa: Estimation of land surface temperature over the Tibetan Plateau using GMS data, *J. Appl. Meteorol.*, Vol. 43, No. 4, 548-561(2004).

Randall, D. A. and D.-M. Pan, 1993: Implementation of the Arakawa-Schubert cumulus parameterization with a prognostic closure. The representation of cumulus convection in numerical models. American Meteorological Society, 137--147.

Slingo, J. M. and coauthors, 1996: Intraseasonal oscillations in 15 atmospheric general circulation models: results from an AMIP diagnostic subproject. Clim. Dynamics, 12, 325--357.

Toth, Z. and E. Kalnay, 1993: Ensemble forecasting at NMC : The generation of pertubations. Bull. Amer. Meteor. Soc., 74, 2317--2330.

Toth, Z. and E. Kalnay, 1997: Ensemble forecasting at NCEP and the breeding method. Mon. Wea. Rev., 125, 3297--3319.

Uchida T., Sugita K. and Ohya Y. （2004）: Evaluation on wind characteristics around a steep simple terrain in a uniform flow, Journal of Wind Engineering, No.100, pp. 35-43.

Tsuyuki, T., 1990: Prediction of the 30-60 day oscillation with JMA global model and its impact on extended-range forecasts. J. Meteor. Soc. Japan, 68, 183--201.

Yasunari, T., 1979: Cloudiness fluctuations associated with the Northern Hemisphere monsoon. J. Meteor. Soc. Japan, 58, 225-229.

異常気象とそれに伴う災害の実態把握と予測に関する研究

河井宏允・岩嶋樹也・石川裕彦・丸山敬・向川均
堀口光章・井口敬雄・荒木時彦

要旨

本報告は，異常気象を引き起こす原因の解明と，それによってもたらされる災害の実態について述べたもので３部からなっている。第１部では，気象庁現業の数値天気予報モデルを用いて，熱帯大気中の季節内振動のアンサンブル予報に適した摂動を生成するように，成長モード育成法の改良を行った結果について述べている。得られた初期摂動は，位相速度が約30 m/sで東進する，対流とは結合しない，東西波数1のKelvin 波と良く似た空間構造を持っていることが示された。摂動の成長率は，中高緯度における傾圧不安定にくらべ大変小さいことがわかった。第2部では，強風特性を明らかにし，強風による被害予測の用に供するために，2004年の台風18号を解析対象として，厳島神社周辺の複雑な地形上における台風通過時強風の再現を数値計算により試みた結果について述べている。地形を再現できる程度の詳細な解析領域を使用した．計算にはメソスケールの気象場を解析できるPSU/NCAR MM5，および，ＬＥＳを用いた狭域スケールの非定常・非線形風況シミュレータRIAM-COMPACTを用いた。第3部では，2005年からデータの取得可能となったFY2Cの衛星画像データの精度を，MTSATのデータと比較することによって検証するとともに，FY2Cデータの補正方法を検討した結果について述べた。

キーワード:異常気象，マダンージュリアン振動，気象庁１カ月予報システム，初期擾乱，数値シミュレーション，強風，複雑地形，台風，MM5，LES，衛星データ解析，FY2C, MTSAT, MODTRAN